

Three-dimensional Bioluminescent Source Reconstruction Method based on Nodes of Adaptive FEM

Chenghu Qin^a, Jie Tian^a, Yujie Lv^a and Wei Yang^a

^aMedical Image Processing Group, Key Laboratory of Complex Systems and Intelligence Science, Institute of Automation Chinese Academy of Sciences, P.O.Box 2728, Beijing, 100080, China

ABSTRACT

As a novel and rapidly growing optical molecular imaging technology, bioluminescence tomography (BLT) can localize and quantify an internal bioluminescent source with the bioluminescent signal on the external surface of a small animal to reveal non-invasive molecular and cellular activities directly. Adaptive finite element method (FEM) based on discretized elements has been introduced into BLT field recently, but the quickly increasing number of subdivided elements will reduce the source reconstruction efficiency greatly along with mesh refinement. In this contribution, a three-dimensional BLT reconstruction method based on nodes of adaptive FEM is developed for determining bioluminescent source distribution to solve the aforementioned problem, which can improve localization of source and enhance the efficiency of reconstruction. Furthermore, BLT is ill-posed for high scattering properties of the biological tissues and the limited boundary detection data. Thus, adequate *a priori* knowledge should be incorporated in this proposed algorithm to reduce the ill-posedness of BLT, such as optical parameters and anatomical structures information of the tissues. Finally, the performance of this reconstruction method is verified with the homogeneous and heterogeneous mouse chest phantoms and Monte Carlo (MC) simulation data. The results show the effectiveness and merits of this tomographic algorithm for BLT.

Keywords: bioluminescence tomography (BLT), diffusion approximation, adaptive finite element method, Monte Carlo, light source reconstruction

1. INTRODUCTION

Optical molecular imaging is a newly emerging and rapidly developing biomedical imaging field in which the modern technologies and instruments are being married to study biological and medical processes as well as diagnosing and managing diseases better.¹⁻³ In comparison with traditional imaging modalities like ultrasound, computed tomography (CT), magnetic resonance imaging (MRI), positron emission tomography (PET) and single photon emission computed tomography (SPECT), optical molecular imaging can not only depict non-invasive *in vivo* cellular and molecular processes selectively and directly, but also obtain functional and spatial information simultaneously with much higher imaging contrast and sensitivity.^{4,5} Fluorescence imaging and bioluminescence imaging (BLI) considered as two typical techniques of optical molecular imaging have been proved to be effective tools for small animal *in vivo* imaging.⁶ However, the nonspecific fluorescence on the skin, food and hair of small animal excited by the external excitation light source will aggravate the background noise and reduce the signal-to-noise ratio (SNR) of measured data. On the contrary, bioluminescence imaging has no background autofluorescence in most tissues, which yields high sensitivity and it can detect as few as several hundred cells *in vivo*.^{7,8}

Bioluminescence imaging employs luciferase enzymes, which can catalyze the biochemical reactions of substrate luciferin with oxygen, ATP and Mg^{2+} to generate bioluminescent photons.⁴ However, bioluminescence imaging is planar and can not reflect the depth information of internal bioluminescent source, so it is used in qualitative research mainly. With the introduction of bioluminescence tomography (BLT), quantitative analyses of the localization and distribution of bioluminescent source in a small animal or a physical phantom become

Further author information: (Send correspondence to Jie Tian)
Jie Tian: E-mail: tian@ieee.org, Telephone: +86 (10)-8261-8465

Medical Imaging 2008: Physiology, Function, and Structure from Medical Images
edited by Xiaoping P. Hu, Anne V. Clough, Proc. of SPIE Vol. 6916, 69161K, (2008)
1605-7422/08/\$18 · doi: 10.1117/12.770215

possible.⁹⁻¹¹ In general, BLT is to reconstruct the internal bioluminescent source with the measured bioluminescent signal on the external surface of a living small animal or a physical phantom, which can be utilized for tumorigenesis studies, cancer diagnosis, gene therapies, metastasis detection, drug discovery and development.^{4, 10, 11} As an emerging and promising optical molecular imaging technique, BLT has become a research focus and an important assistant tool for detecting and studying specific biomolecular processes in living cells. However, BLT is severely ill-posed for high scattering properties of the biological tissues and the limited and noisy boundary detection data. Therefore, adequate *a priori* information including the tissues optical parameters and three-dimensional anatomical structures should be incorporated to reduce the ill-posed nature of BLT, and regularization method is also employed for the uniqueness and stability of the BLT solution.¹²

Considering the balance between reconstruction precision and computational cost, adaptive finite element method (FEM) based on discretized elements has been developed for BLT recently.¹³⁻¹⁵ To a certain extent, the finer the subdivided mesh becomes, the larger the number of formed elements are. Therefore, the efficiency of bioluminescent source reconstruction is reduced greatly. Furthermore, the number of vertices is much larger than that of elements when a given region is divided into tetrahedra. On the other hand, the object of optical molecular imaging is to observe the biological processes *in vivo* at the molecular and cellular levels, so the volume of bioluminescent source in the phantom or small animal is very tiny and approximated to a node compared with the whole shape. However, the final reconstruction result of adaptive FEM based on discretized elements is a volumetric subdomain. For the above issues, a three-dimensional bioluminescent source reconstruction method based on nodes of adaptive FEM is developed and validated in this paper.

The paper is organized as follows. The next section introduces the proposed source reconstruction algorithm for BLT. In section 3, the performance of this method is tested. Finally, a discussion of relevant issues and conclusion are provided.

2. METHODS

2.1 Diffusion approximation and Robin boundary condition

Bioluminescent photons transport in the biological tissue can be accurately depicted by the radiative transfer equation (RTE), but it is computationally expensive in practical bioluminescence imaging for its integro-differential nature. Thus, the mathematical model widely adopted in bioluminescence imaging is diffusion equation approximated from RTE for the high scattering property of the biological tissue.¹⁶ Furthermore, when the bioluminescence imaging experiment is carried out in a totally dark environment, the propagation of bioluminescent photons in the biological tissue can be well modeled by steady-state diffusion equation and Robin boundary condition because the internal bioluminescent source is continuously on during the measurement:¹⁷⁻²⁰

$$-\nabla \cdot (D(\mathbf{x})\nabla\Phi(\mathbf{x})) + \mu_a(\mathbf{x})\Phi(\mathbf{x}) = S(\mathbf{x}) \quad (\mathbf{x} \in \Omega) \quad (1)$$

$$\Phi(\mathbf{x}) + 2A(\mathbf{x}; n, n')D(\mathbf{x})(\mathbf{v}(\mathbf{x}) \cdot \nabla\Phi(\mathbf{x})) = 0 \quad (\mathbf{x} \in \partial\Omega) \quad (2)$$

where Ω and $\partial\Omega$ are the given domain and the corresponding boundary respectively; $\Phi(\mathbf{x})$ represents the photon density [*Watts/mm²*] at location \mathbf{x} ; $S(\mathbf{x})$ denotes the bioluminescent source density [*Watts/mm³*]; $\mu_a(\mathbf{x})$ is the absorption coefficient [*mm⁻¹*]; $D(\mathbf{x}) = 1/(3(\mu_a(\mathbf{x}) + (1-g)\mu_s(\mathbf{x})))$ is the optical diffusion coefficient, $\mu_s(\mathbf{x})$ the scattering coefficient [*mm⁻¹*], and g the anisotropy parameter; $\mathbf{v}(\mathbf{x})$ is the unit outer normal on $\partial\Omega$; $A(\mathbf{x}; n, n')$ is a function to incorporate a mismatch between the refractive indices n within Ω and n' in the surrounding medium. Moreover, the refractive index of the surrounding medium n' is close to 1.0 if the bioluminescence imaging experiment is performed in air, and $A(\mathbf{x}; n, n')$ can be approximated further as follows:

$$A(\mathbf{x}; n, n') \approx \frac{1 + R(\mathbf{x})}{1 - R(\mathbf{x})} \quad (3)$$

where $R(\mathbf{x})$ can be approximately depicted:²¹

$$R(\mathbf{x}) \approx -1.4399n^{-2} + 0.7099n^{-1} + 0.6681 + 0.0636n \quad (4)$$

In our study, the measured outgoing flux density $Q(\mathbf{x})$ on $\partial\Omega$ is:²¹

$$Q(\mathbf{x}) = -D(\mathbf{x})(\mathbf{v} \cdot \nabla\Phi(\mathbf{x})) = \Phi(\mathbf{x})/(2A(\mathbf{x}; n, n')) \quad (5)$$

2.2 Algorithm

Based on Galerkin method and Gauss theory, Eqs. (1)-(2) can be transformed to the following weak form:²¹

$$\int_{\Omega} \left(D(\mathbf{x})(\nabla\Phi(\mathbf{x})) \cdot (\nabla\Psi(\mathbf{x})) + \mu_a(\mathbf{x})\Phi(\mathbf{x})\Psi(\mathbf{x}) \right) d\mathbf{x} + \int_{\partial\Omega} \frac{1}{2A(\mathbf{x}; n, n')} \Phi(\mathbf{x})\Psi(\mathbf{x}) d\mathbf{x} = \int_{\Omega} S(\mathbf{x})\Psi(\mathbf{x}) d\mathbf{x} \quad (6)$$

where $\Psi(\mathbf{x})$ denotes an arbitrary test function and belongs to Sobolev space $H^1(\Omega)$.

According to the generalized finite element method, the region of interest Ω can be discretized with N_e nonoverlapping subdomains (elements) and N_n vertex nodes, satisfying $\Omega = \cup_{l=1}^{N_e} \Omega^{(l)}$. To the best of our knowledge, the system matrices are constructed based on elements in the former adaptive finite element methods for bioluminescence tomography, and their efficiencies are reduced greatly with the mesh evolution because N_e is much larger than N_n when the domain Ω is divided into tetrahedral elements. Moreover, the final reconstruction result of adaptive finite element method based on discretized elements is a volumetric tetrahedron, so it is difficult to reconstruct a very small bioluminescent source which can be approximated as point light source. Therefore, the system matrices are formed based on nodes of adaptive finite element method in the proposed method to resolve the above problem. Firstly, the photon density $\Phi(\mathbf{x})$ and the bioluminescent source density $S(\mathbf{x})$ can be approximated with their corresponding nodal values:

$$\Phi(\mathbf{x}) \approx \sum_{i=1}^{N_n} \phi_i \psi_i(\mathbf{x}) \quad (7)$$

$$S(\mathbf{x}) \approx \sum_{i=1}^{N_n} s_i \psi_i(\mathbf{x}) \quad (8)$$

where ϕ_i and s_i are the nodal value of $\Phi(\mathbf{x})$ and $S(\mathbf{x})$ on the i -th node respectively; $\psi_i(\mathbf{x})$ is the nodal shape function with support over all elements which have a common vertex node, and satisfies the delta function property: $\psi_i(\mathbf{x}_j) = \delta_{ij}$.

Incorporating Eqs. (7) and (8) with Eq. (6), the ill-conditioned linear matrix equation can be established as follows:

$$(K + C + B)\Phi = M\Phi = FS \quad (9)$$

where the components of the matrices K , C , B and F are obtained by

$$\begin{cases} k_{ij} = \int_{\Omega} D(\mathbf{x})(\nabla\psi_i(\mathbf{x})) \cdot (\nabla\psi_j(\mathbf{x})) d\mathbf{x} \\ c_{ij} = \int_{\Omega} \mu_a(\mathbf{x})\psi_i(\mathbf{x})\psi_j(\mathbf{x}) d\mathbf{x} \\ b_{ij} = \int_{\partial\Omega} \psi_i(\mathbf{x})\psi_j(\mathbf{x}) / (2A(\mathbf{x}; n, n')) d\mathbf{x} \\ f_{ij} = \int_{\Omega} \psi_i(\mathbf{x})\psi_j(\mathbf{x}) d\mathbf{x} \end{cases} \quad (10)$$

Φ and S are N_n -dimensional vectors: $\Phi = (\phi_1, \phi_2, \dots, \phi_{N_n})^T$, $S = (s_1, s_2, \dots, s_{N_n})^T$; M and F are N_n order square matrices; furthermore, M is a symmetric positive definite and invertible matrix. Therefore, Eq. (9) can be further transformed as:

$$\Phi = M^{-1}FS \quad (11)$$

Considering the boundary measured data Φ^{meas} and the permissible source region S^p of the given domain, $M^{-1}F$ can be simplified to a $N_b \times N_p$ order matrix A , which can be obtained through retaining the columns corresponding to S^p in $M^{-1}F$ and reserving the rows of $M^{-1}F$ corresponding to Φ^{meas} :

$$\Phi^{meas} = AS^p \quad (12)$$

where N_b is the number of boundary measured points and N_p is the number of discretized nodes in the permissible source region. To compute bioluminescent source distribution and keep the uniqueness and stability of the BLT solution, the optimization objective function is defined using Tikhonov regularization method:

$$\min_{0 \leq S^p \leq S^{sup}} \Theta(S^p) = \left\{ \|AS^p - \Phi^{meas}\|_{\Lambda} + \lambda\eta(S^p) \right\} \quad (13)$$

where S^{sup} is the upper bound of the bioluminescent source density; Λ is the weight matrix, $\|V\|_{\Lambda} = V^T \Lambda V$; λ is the regularization parameter; $\eta(X) = X^T X$ is the penalty function.

A modified Newton method and a specific Hessian matrix are utilized to settle the above minimization problem (13) with simple bounds for a appropriate regularization parameter, and then the final localization and density of the internal bioluminescent source can be determined.²² The main steps are described as follows. From a given starting point S^k , an active set I can be built, which contains the indices of the variables at their bounds. If a variable is not in the active set, it can be called as “free variable”, and then the search direction d^k for the free variables is computed with the formula:

$$d^k = -H^{-1}g^k \quad (14)$$

where H is the Hessian matrix and g^k is the gradient evaluated at S^k . A new point S^{k+1} can be found by linear search method:

$$S^{k+1} = S^k + \alpha d^k \quad \alpha \in (0, 1] \quad (15)$$

such that

$$f(S^{k+1}) \leq f(S^k) + \beta g^T d^k \quad \beta \in (0, 0.5) \quad (16)$$

Finally, a specified gradient tolerance is used as the stopping criterion to evaluate whether the optimality should be terminated. The above process should be repeated by changing search direction until stopping criterion is met, and then the optimal bioluminescent source distribution can be calculated.

The global and the local *a posteriori* discretization errors based on adaptive technology are employed to improve location and quantification of the bioluminescent source further after optimization.²³ The global error is used to stop the whole reconstruction program when the requested precision is reached, and the local error is utilized to determine elements which will be refined. Then, the reconstruction algorithm will be executed again with the refined mesh until termination conditions are met.

3. RESULTS

In the bioluminescence imaging simulation experiment, cylindrical homogeneous and heterogeneous mouse chest physical phantoms with 10mm radius and 30mm height were used to validate the feasibility of this proposed algorithm successively, as shown in Fig. 1(a) and 2(a) respectively. The homogeneous phantom only consisted of one resinous material to represent muscle, and the heterogeneous one comprised five kinds of simulation tissues: muscle, lungs, heart, bone and liver. The optical parameters of these tissues can be obtained from the literature,²⁴ as listed in Table 1.

Table 1. Optical parameters for the homogeneous and heterogeneous phantoms

Material	Muscle	Lung	Heart	Bone	Liver
$\mu_a(mm^{-1})$	0.035	0.35	0.2	0.04	0.035
$\mu_s(mm^{-1})$	3.0	23.0	16.0	35.0	6.0
g	0.98	0.94	0.85	0.925	0.97

Monte Carlo (MC) method, regarded as “Gold Standard”, is rigorous, flexible and powerful to study photon transport phenomena in the turbid tissue, which has been used for both diagnostic and therapeutic applications of lasers and other optical sources.^{25,26} Based on MC method, molecular optical simulation environment (MOSE) has been developed by our group, which is a forward model for bioluminescent photon propagation in order to simulate bioluminescent phenomena in the small animal imaging. In addition, bioluminescent signals around the small animal or the physical phantom can be predicted with MOSE.²⁷ Firstly, object file format (.off) files

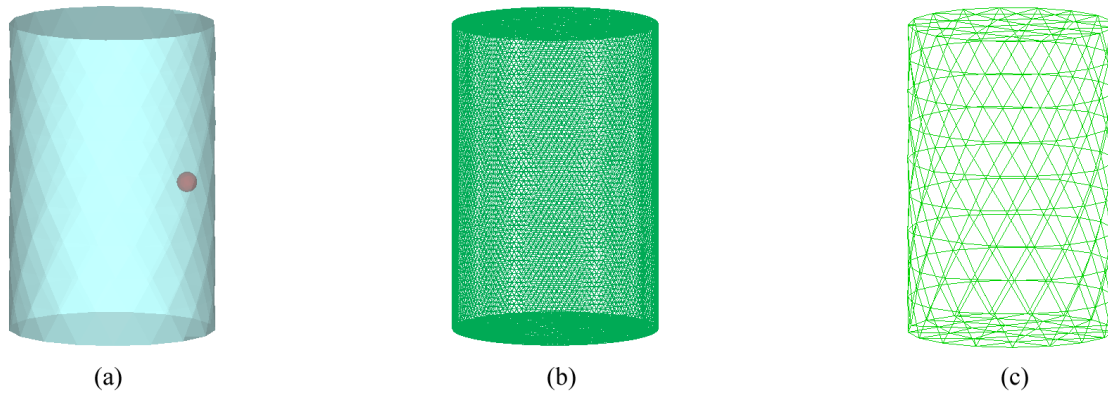


Figure 1. The homogeneous phantom. (a) The homogeneous phantom with a spherical light source; (b) The discretized mesh used in the simulation of the forward model; (c) The first level mesh used in the developed algorithm.

were inputted to MOSE for generating the synthetic data, which could be obtained by discretizing the above phantoms. The homogeneous phantom was discretized into 11512 vertices and 23020 triangular elements, and the heterogeneous phantom was divided into 17146 nodes and 34268 surface elements for MOSE simulation herein, as shown in Fig. 1(b) and 2(b). In the homogeneous phantom, an embedded spherical source with 1.0mm radius and $0.477\text{nano} - \text{Watts}/\text{mm}^3$ power density was centered at $(-8.0, 0.0, 15.0)$. In the heterogeneous phantom, a spherical source of 1.0mm radius and $0.238\text{nano} - \text{Watts}/\text{mm}^3$ power density was placed at $(-3.0, 5.0, 15.0)$ in the right lung. Using MOSE, the bioluminescent light exitance maps on the surface of the homogeneous and heterogeneous physical phantoms could be simulated, as shown in Fig. 3(a) and 3(b).

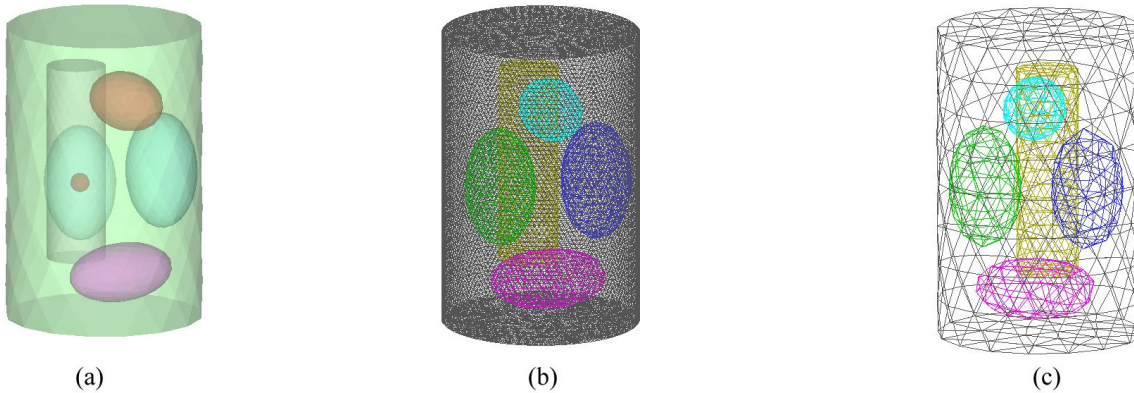


Figure 2. The heterogeneous mouse chest phantom. (a) The heterogeneous phantom with a light source in the right lung; (b) The subdivided mesh of the heterogeneous phantom utilized in MOSE; (c) The initial mesh used in the proposed algorithm.

In bioluminescent source reconstruction, the maximal element diameters of the aforementioned homogeneous and heterogeneous phantoms were 2.5mm and 4.0mm respectively in the initial mesh, as shown in Fig. 1(c) and 2(c). The bioluminescent source reconstruction results of the homogeneous and heterogeneous phantoms are shown in Fig. 4(a)-(c). In the homogeneous phantom, the center and density of reconstructed source was $(-9.89, 0.54, 15.07)$ and $0.464\text{nano} - \text{Watts}/\text{mm}^3$ respectively. In the heterogeneous phantom, the center of reconstructed source was located at $(-3.08, 5.00, 15.61)$ and the reconstructed source power density was $0.224\text{nano} - \text{Watts}/\text{mm}^3$. The corresponding quantitative comparisons between the real sources and the calculation results are shown in Table 2, and RE in the table represents the relative error between the actual source and the reconstructed result, which can be computed with the formula $RE = |S_{real} - S_{recons}|/S_{real}$, S_{real} the real

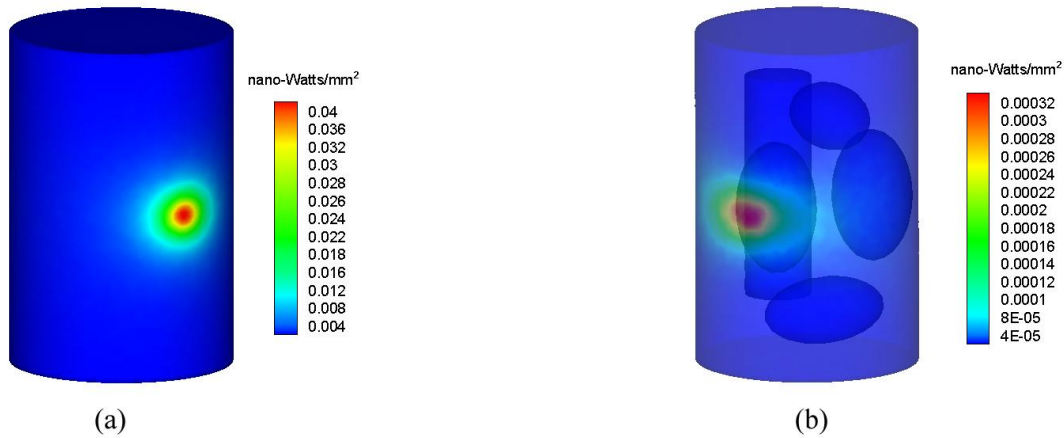


Figure 3. Bioluminescent signals around the phantoms simulated by MOSE. (a) The surface light power of the homogeneous phantom; (b) The light exittance map on the surface of the heterogeneous phantom.

internal bioluminescent source, and S_{recons} the reconstructed source. Furthermore, the efficiencies of adaptive finite element method based on elements and this proposed algorithm were compared using the same regularization parameter and discretized mesh, which are summarized in Table 3. When the bioluminescent source was reconstructed in the homogeneous phantom, 146.41s were needed to complete optimization when adaptive finite element method based on elements was used. However, only 1.02s were spent when using the proposed algorithm. When we reconstructed the internal source in the heterogeneous phantom with the developed method in this paper, only 623.05s were required for minimization. By contrast, the optimization time ($> 24hours$) was already beyond our endurance when adaptive finite element method based on element was employed.

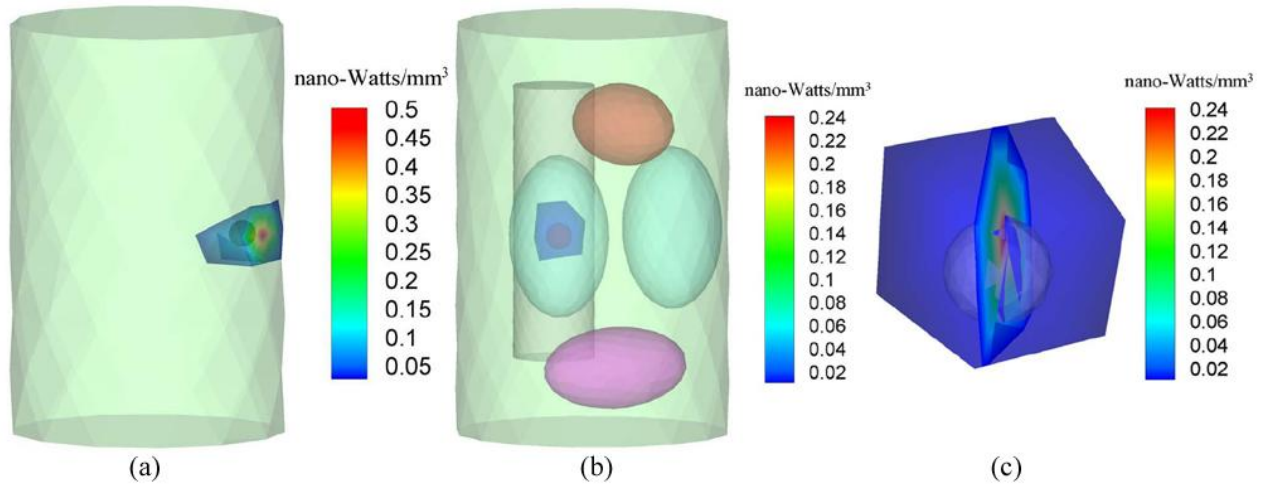


Figure 4. Bioluminescent source reconstructed results. (a) The reconstructed result of the homogeneous phantom; (b) The reconstructed result of the heterogeneous phantom; (c) The magnified slice image of (b).

Table 2. Comparison between the actual and reconstructed sources

Phantom	Actual position	Reconstructed position	Actual density	Reconstructed density	RE
Homogeneous	(-8.0, 0.0, 15.0)	(-9.89, 0.54, 15.07)	0.477	0.464	2.7%
Heterogeneous	(-3.0, 5.0, 15.0)	(-3.08, 5.00, 15.61)	0.238	0.224	5.9%

Table 3. Efficiencies comparison between adaptive FEM based on elements and the proposed algorithm

Phantom	The number of nodes	The number of elements	Optimization time with adaptive FEM based on elements	The proposed algorithm
Homogeneous	239	722	146.41s	1.02s
Heterogeneous	842	4185	> 24hours	623.05s

4. DISCUSSION AND CONCLUSION

Adaptive finite element method (FEM) based on discretized elements has already been utilized in bioluminescence tomography (BLT) to improve localization and quantification of the internal bioluminescent source. However, with the mesh refinement, the efficiency of this algorithm will be debased greatly for the huge system matrices. Furthermore, the volume of reconstructed result is too large to reflect the nature of molecular imaging. Therefore, a fast three-dimensional bioluminescent source reconstruction method based on discretized nodes of adaptive FEM is developed in this contribution, which can reduce the time and memory cost of the tomographic algorithm.

Finally, the proposed method has been tested using the homogeneous and heterogeneous mouse chest phantoms to demonstrate the efficiency and feasibility of the algorithm. There were some deviations between the computed results and the actual source locations because every reconstructed source was a point in this method. Furthermore, the source intensities were reconstructed with very small relative errors. The future work will further reduce the information of discretized elements in bioluminescent source reconstruction and the corresponding results will be reported later.

5. ACKNOWLEDGEMENTS

This paper is supported by the Project for the National Key Basic Research and Development Program (973) under Grant No. 2006CB705700, Changjiang Scholars and Innovative Research Team in University (PCSIRT) under Grant No. IRT0645, CAS Hundred Talents Program, CAS scientific research equipment develop program (YZ0642, YZ200766), 863 program under Grant No. 2006AA04Z216, the Joint Research Fund for Overseas Chinese Young Scholars under Grant No. 30528027, the National Natural Science Foundation of China under Grant No. 30672690, 30600151, 30500131, 60532050, Beijing Natural Science Fund under Grant No. 4051002, 4071003.

REFERENCES

1. C. H. Contag and M. H. Bachmann, "Advances in bioluminescence imaging of gene expression," *Annual Review of Biomedical Engineering* **4**, pp. 235–260, 2002.
2. S. Bhaumik and S. S. Gambhir, "Optical imaging of renilla luciferase reporter gene expression in living mice," *Proceedings of the National Academy of Sciences USA* **99**, pp. 377–382, 2002.
3. T. F. Massoud and S. S. Gambhir, "Molecular imaging in living subjects: seeing fundamental biological processes in a new light," *Genes and development* **17**, pp. 545–580, 2003.
4. V. Ntziachristos, J. Ripoll, L. Wang, and R. Weissleder, "Looking and listening to light: the evolution of whole-body photonic imaging," *Nat. Biotech.* **23**, pp. 313–320, 2005.
5. W. Cong, G. Wang, D. Kumar, Y. Liu, M. Jiang, L. Wang, E. Hoffman, G. McLennan, P. McCray, J. Zabler, and A. Cong, "Practical reconstruction method for bioluminescence tomography," *Optics Express* **13**, pp. 6756–6771, 2005.
6. P. R. Contag, I. N. Olomu, D. K. Stevenson, and C. H. Contag, "Bioluminescent indicators in living mammals," *Nat. Med.* **4**, pp. 245–247, 1998.
7. M. Edinger, Y. A. Cao, M. R. Verneris, M. H. Bachmann, C. H. Contag, and R. S. Negrin, "Revealing lymphoma growth and the efficacy of immune cell therapies using *in vivo* bioluminescence imaging," *Blood* **101**, pp. 640–648, 2003.
8. B. W. Rice, M. D. Cable, and M. B. Nelson, "*In vivo* imaging of light-emitting probes," *Journal of Biomedical Optics* **6**, pp. 432–440, 2001.

9. G. Wang, E. A. Hoffman, G. McLennan, L. V. Wang, M. Suter, and J. F. Meinel, "Development of the first bioluminescence CT scanner," *Radiology* **229**, p. 566, 2003.
10. W. Cong, D. Kumar, Y. Liu, A. Cong, and G. Wang, "A practical method to determine the light source distribution in bioluminescent imaging," *Proc. SPIE* **5535**, pp. 679–686, 2004.
11. G. Wang, H. Shen, W. Cong, S. Zhao, and G. WeiWei, "Temperature-modulated bioluminescence tomography," *Optics Express* **14**, pp. 7852–7871, 2006.
12. G. Wang, Y. Li, and M. Jiang, "Uniqueness theorems in bioluminescence tomography," *Med. Phys.* **31**, pp. 2289–2299, 2004.
13. Y. Lv, J. Tian, W. Cong, G. Wang, J. Luo, W. Yang, and H. Li, "A multilevel adaptive finite element algorithm for bioluminescence tomography," *Optics Express* **14**, pp. 8211–8223, 2006.
14. D. Wang, X. Song, and J. Bai, "Adaptive-mesh-based algorithm for fluorescence molecular tomography using an analytical solution," *Optics Express* **15**, pp. 9722–9730, 2007.
15. Y. Lv, J. Tian, W. Cong, G. Wang, W. Yang, C. Qin, and M. Xu, "Spectrally resolved bioluminescence tomography with adaptive finite element: methodology and simulation," *Phys. Med. Biol.* **52**, pp. 4497–4512, 2007.
16. A. P. Gibson, J. C. Hebden, and S. R. Arridge, "Recent advances in diffuse optical imaging," *Phys. Med. Biol.* **50**, pp. R1–R43, 2005.
17. V. Ntziachristos, C. B. C. Tung, and R. Weissleder, "Fluorescence molecular tomography resolves protease activity *in vivo*," *Nat. Med.* **8**, pp. 757–760, 2002.
18. R. Schultz, J. Ripoll, and V. Ntziachristos, "Experimental fluorescence tomography of tissues with noncontact measurements," *IEEE Trans. Med. Imag.* **23**, pp. 492–500, 2004.
19. J. Ripoll, D. Yessayan, G. Zacharakis, and V. Ntziachristos, "Experimental determination of photon propagation in highly absorbing and scattering media," *J. Opt. Soc. Am. A* **22**, pp. 546–551, 2005.
20. S. R. Arridge, M. Schweiger, M. Hiraoka, and D. T. Delpy, "A finite element approach for modeling photon transport in tissue," *Med. Phys.* **20**, pp. 299–309, 1993.
21. M. Schweiger, S. R. Arridge, M. Hiraoka, and D. T. Delpy, "The finite element method for the propagation of light in scattering media: Boundary and source conditions," *Med. Phys.* **22**, pp. 1779–1792, 1995.
22. P. E. Gill, W. Murray, and M. Wright, *Practical Optimization*, Academic Press, New York, 1981.
23. A. Joshi, W. Bangerth, and E. M. Sevick-Muraca, "Adaptive finite element based tomography for fluorescence optical imaging in tissue," *Optics Express* **12**, pp. 5402–5417, 2004.
24. G. Alexandrakis, F. R. Rannou, and A. F. Chatziioannou, "Tomographic bioluminescence imaging by use of a combined optical-PET (OPET) system: a computer simulation feasibility study," *Phys. Med. Biol.* **50**, pp. 4225–4241, 2005.
25. E. Margallo-Balbás and P. J. French, "Shape based Monte Carlo code for light transport in complex heterogeneous tissues," *Optics Express* **15**, pp. 14086–14098, 2007.
26. L. H. Wang, S. L. Jacques, and L. Q. Zheng, "MCML-Monte Carlo modeling of photon transport in multilayered tissues," *Comput. Meth. Prog. Biomed.* **47**, pp. 131–146, 1995.
27. H. Li, J. Tian, F. Zhu, W. Cong, L. Wang, E. Hoffman, and G. Wang, "A mouse optical simulation environment (MOSE) to investigate bioluminescent phenomena in the living mouse with Monte Carlo method," *Acad. Radiol.* **11**, pp. 1029–1038, 2004.